Weierstraß-Institut

für Angewandte Analysis und Stochastik

Leibniz-Institut im Forschungsverbund Berlin e. V.

p-Laplace thermistor modeling of electrothermal feedback in organic semiconductors

Matthias Liero [1], Thomas Koprucki [1], Axel Fischer [2],

Reinhard Scholz [2], Annegret Glitzky [1]

[1] Weierstrass Institute
Mohrenstraße 39
10117 Berlin
Germany
E-Mail: annegret.glitzky@wias-berlin.de
thomas.koprucki@wias-berlin.de
matthias.liero@wias-berlin.de

[2] Institut für Angewandte Photophysik (IAPP)
Technische Universität Dresden
George-Bähr-Straße 1
01069 Dresden
Germany
E-Mail: axel.fischer@iapp.de
reinhard.scholz@iapp.de

Abstract

In large-area Organic Light-Emitting Diodes (OLEDs) spatially inhomogeneous lumi-
nance at high power due to inhomogeneous current flow and electrothermal feedback
can be observed. To describe these self-heating effects in organic semiconductors we
present a stationary thermistor model based on the heat equation for the tempera-
ture coupled to a p-Laplace-type equation for the electrostatic potential with mixed
boundary conditions. The p-Laplacian describes the non-Ohmic electrical behavior
of the organic material. Moreover, an Arrhenius-like temperature dependency of the
electrical conductivity is considered.

We introduce a finite-volume scheme for the system and discuss its relation to
recent network models for OLEDs. In two spatial dimensions we derive a priori esti-
mates for the temperature and the electrostatic potential and prove the existence of
a weak solution by Schauder's fixed point theorem.

1   Introduction

Light-emitting diodes are one of the main application areas of organic semiconductors.
Organic Light-Emitting Diodes (OLEDs) are not only used in displays of smartphones
or flat screens, but also occur in intelligent lighting applications. However, there still
exist many technical issues in the development of flat OLED lighting panels, e.g. avoiding
a spatially non-uniform light emission at high brightness. Therefore, accurate methods
for modeling the specific electronic properties of the OLED layer and for the thermal
management of the whole large-area lighting panel are needed to achieve a temperature-
stable operation, see [1, 29].

For carbon-based, organic semiconductor materials the well-known Arrhenius law ap-
plies [13]: The electrical conductivity increases with rising temperature. At constant
voltage, the electric current as well as the power dissipation increases, causing a positive
feedback loop which continuously heats up the structure. Often experiments of this kind
lead to the destruction of the device by thermal breakdown if the heat cannot be dispersed
into the environment, see [12]. Devices strongly sensible to temperature and thus resulting
in such self-amplification effects are called thermistors ([24, Ch. 8]) and can be used as
sensors or in power electronics.

A thermistor-like behavior of organic semiconductors induced by self-heating has been
demonstrated for the organic semiconductor C_{60} in [13] and for organic materials used as
active layers in OLEDs in [11]. Moreover, in large-area OLEDs self-heating leads to spa-
tially inhomogeneous current and temperature distributions resulting in inhomogeneities
in the luminance for higher light intensities. Especially, in lighting panels the area becomes
spotty, see [21, 1].

The approaches for electrothermal modeling of OLED devices in the literature mainly go
in two directions. One possibility is the description of current and heat flow by a coupled
system of partial differential equations, where the influence of the organic layer is reduced
to empirical characteristics (see [25, 26]). For example, the SUNRED algorithm ([22, 18])
combines finite difference models for thermal and electrical properties of the electrode and
substrate material layers with the nonlinear characteristics of the organic substructure.
The other way to describe the electrothermal behavior of OLED devices are electrothermal

equivalent circuits (as in [11]), where the organic substructure is represented by a finite array of thermistors. The Joule heat produced by the electrical network is balanced by a related thermal network.

In this paper we present a full PDE model for the electrothermal description of organic semiconductor devices including their stack, which contains additionally the contacting by the metal and Indium Tin Oxide (ITO) layers as well as the substrate material, see Fig. 2. The model complexity includes an Arrhenius-like temperature dependent conductivity law for materials with non-Ohmic behavior, which is characteristic for organic semiconductors. This PDE modeling approach gives much more flexibility concerning variations in geometry and material composition than network models. Moreover, our model contains also a PDE-type description of the active organic zone whereas in the other above mentioned PDE simulation approach the organic layer is reduced to the information from empirical characteristics.

In Subsection 2.1 we summarize the self-heating theory in the spatially homogeneous situation which leads to S-shaped current-voltage curves with regions of Negative Differential Resistance (NDR). Subsection 2.2 motivates the appearance of special inhomogeneities in large-area OLEDs induced by the sheet resistance of ITO top contacts. To illustrate the influence of such inhomogeneities, the behavior of a chain of thermistors coupled to a thermal network is studied, revealing interesting switching effects due to NDR.

In Section 3 a spatially resolved model for real devices based on coupled partial differential equations for heat and current flow is presented. It is of thermistor model type and contains a p-Laplacian operator, where $p > 2$ applies for organic materials. In contrast to multi-physics circuit models, describing coupled electrical and thermal networks (see [11]), our PDE-based thermistor model with non-Ohmic current-voltage laws is expected to be better suited for a realistic description of the geometry of the whole device. A finite-volume discretization for the thermistor system is introduced in Subsection 3.2. In particular, we show in Subsection 3.3 that the circuit model can be recovered from this scheme by using special grids.

Section 4 is devoted to the analytical investigation of the stationary p-Laplace thermistor model, $p > 2$, in space dimension two. We give a weak formulation of the problem, show a priori bounds for possible solutions (Theorem 4.1) and verify the existence of at least one weak solution of the problem by means of Schauder's fixed point theorem (see Theorem 4.2). In particular, a crucial point in the proof is that higher regularity of the electrostatic potential has to be shown. The paper closes with conclusions, generalizations, remarks, and open problems collected in Section 5.

2 From homogeneous self-heating theory to spatially resolved effects in organic thin film devices

2.1 Special electrothermal effects in organic semiconductors

In this subsection we briefly summarize the self-heating theory in the spatially homogeneous situation as presented in [13]. The charge transport in organic semiconductors occurs by hopping of electrons between discrete energy levels of molecular sites nearby.
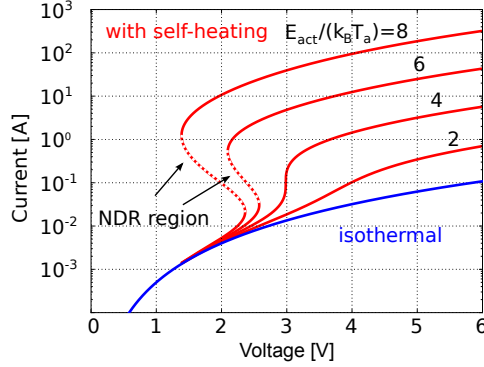
Figure 1: Self-consistent current-voltage characteristics for different activation energies (red). For $E_{\mathrm{act}} > 4k_{\mathrm{B}}T_a$ they show S-shaped NDR (red dashed). Blue: Isothermal current-voltage curve with $\alpha = 3$.

These energy states are Gaussian distributed with variance σ. The dependence of the mobility on the temperature T resulting from the disorder σ can be approximated by an Arrhenius law with an activation energy $E_{\mathrm{act}} = 2C\sigma^2/(k_{\mathrm{B}}T)$ (k_{B} Boltzmann's constant, $C \approx 0.4$), see [27]. The strong increase of the carrier mobility with the temperature leads to self-amplification of the current and to strong self-heating effects at large currents.

For the study of self-heating by a thermally activated conductivity in a spatially homogenous situation, an isothermal current-voltage relation of the device given by a power law

$$I_{\mathrm{iso}}(V, T) = I_{\mathrm{ref}}\Big(\frac{V}{V_{\mathrm{ref}}}\Big)^{\alpha} F(T), \quad \alpha > 0, \tag{2.1}$$

and a conductivity factor $F(T)$ resulting from an Arrhenius law

$$F(T) = \exp\Big[-\frac{E_{\mathrm{act}}}{k_{\mathrm{B}}}\Big(\frac{1}{T} - \frac{1}{T_a}\Big)\Big] \tag{2.2}$$

has been considered in [13]. Here, V_{ref} and I_{ref} denote reference values for voltage and current, respectively, and T_a is the ambient temperature. In the homogeneous steady states of the device the dissipated Joule power VI_{iso} is equal to the heat loss $\frac{1}{\Theta_{\mathrm{th}}}(T - T_a)$ to the surrounding described by the thermal resistance Θ_{th},

$$\frac{1}{\Theta_{\mathrm{th}}}(T - T_a) = V_{\mathrm{ref}}I_{\mathrm{ref}}\Big(\frac{V}{V_{\mathrm{ref}}}\Big)^{\alpha+1} F(T). \tag{2.3}$$

From (2.1) and (2.3) the self-consistent current-voltage curve $(V(T), I(T))$ including self-heating parameterized by $T \geq T_a$ is obtained, see [13].

The red curves in Fig. 1 show calculated self-consistent current-voltage curves for an isothermal current-voltage characteristic ($\alpha = 3$) and different activation energies. For $E_{\mathrm{act}} > 4k_{\mathrm{B}}T_a$, a region of negative differential resistance (NDR), $\frac{\mathrm{d}V}{\mathrm{d}I} < 0$ appears, see [24]. Usual values of the disorder parameter σ in organic semiconductor materials of 2 to 6 $k_{\mathrm{B}}T_a$ give activation energies sufficiently high for the occurrence of NDR regions.
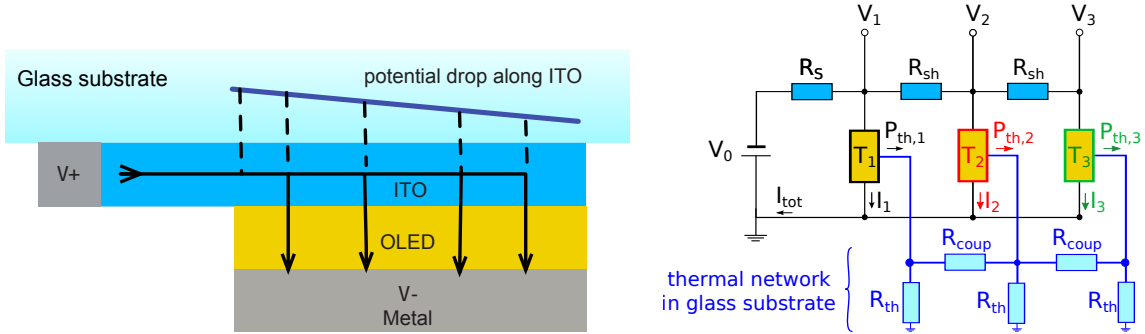
Figure 2: Left: Schematic diagram of current paths and potential drop along the anode contact (ITO) for an OLED with crossbar contacts. Right: Equivalent circuit for SPICE simulation of a 3-thermistor chain.

Along the S-shaped current-voltage characteristics, two stable branches exist: an 'ON' state with high conductivity and an 'OFF' state with low conductivity, whereas the intermediate region of NDR is unstable (dashed red lines in Fig. 1). This behavior has been experimentally demonstrated for a C_{60} device with small active area in [13].

For real devices, an additional constant series resistance R_S resulting from the electrode resistance and the measurement setup has to be added in series to the S-NDR element. If R_S is sufficiently large, thermal switching of the whole circuit is suppressed [13].

2.2   Switching effects in large-area thin film devices

For OLEDs, the optically transparent top contact is often realized using ITO which has a considerably high electrical resistance compared to metals. In particular, for large-area devices this results in a voltage drop along current paths through the ITO contact, see Fig. 2 left. For the typical crossbar contact geometry used for OLEDs this voltage drop leads to a spatial variation of the effective applied voltage across the active OLED layer between ITO and metal contacts, see the left panel in Fig. 2. Note that Fig. 2 (left and right) and Fig. 4 have the same color coding for the different materials (ITO, organic material, metal, and glass substrate).

Therefore, the application of spatially homogeneous models is no longer justified. OLED lighting panels nowadays have a width in the range of 10 to 20 cm and show an inhomogeneous spatial distribution of current and light intensity at higher power.

As a guiding example for the effects present in the spatially resolved situation we briefly discuss the ideas in [11] and introduce an equivalent circuit consisting of three electrically coupled thermistors which are coupled to a thermal network as given in Fig. 2 right. Such problems can be solved with network simulators, e.g. SPICE, which fully reproduce thermistor-like behavior as shown in [17]. We discuss the two different cases (a) without and (b) with thermal coupling by thermal resistances R_{coup} resulting in the diagrams in the first and second row, respectively, in Fig. 3. Note that the characteristics in black, red, and green correspond to the black, red, and green thermistors in Fig. 2 right. Denoting by V_i, I_i the voltage and current of the ith thermistor and by V_{ext} the externally applied

voltage the ith differential resistance is obtained by

$$\frac{\mathrm{d}V_i}{\mathrm{d}I_i} = \frac{\mathrm{d}V_i}{\mathrm{d}V_{\mathrm{ext}}}\left(\frac{\mathrm{d}I_i}{\mathrm{d}V_{\mathrm{ext}}}\right)^{-1}.$$

The following operation modes can be observed:

$\frac{\mathrm{d}V_i}{\mathrm{d}V_{\mathrm{ext}}} > 0,\ \frac{\mathrm{d}I_i}{\mathrm{d}V_{\mathrm{ext}}} > 0$	$\frac{\mathrm{d}V_i}{\mathrm{d}V_{\mathrm{ext}}} < 0,\ \frac{\mathrm{d}I_i}{\mathrm{d}V_{\mathrm{ext}}} > 0$	$\frac{\mathrm{d}V_i}{\mathrm{d}V_{\mathrm{ext}}} < 0,\ \frac{\mathrm{d}I_i}{\mathrm{d}V_{\mathrm{ext}}} < 0$
I: normal mode	II: S-NDR	III: switched back

Fig. 3 gives the following results: In the cases (a) and (b) all thermistors are in normal mode for small applied voltages V_{ext}.

In case (a) without any thermal coupling between the thermistors, the thermistor T_1 (black) closest to the contact starts to show S-NDR upon the transition of a critical
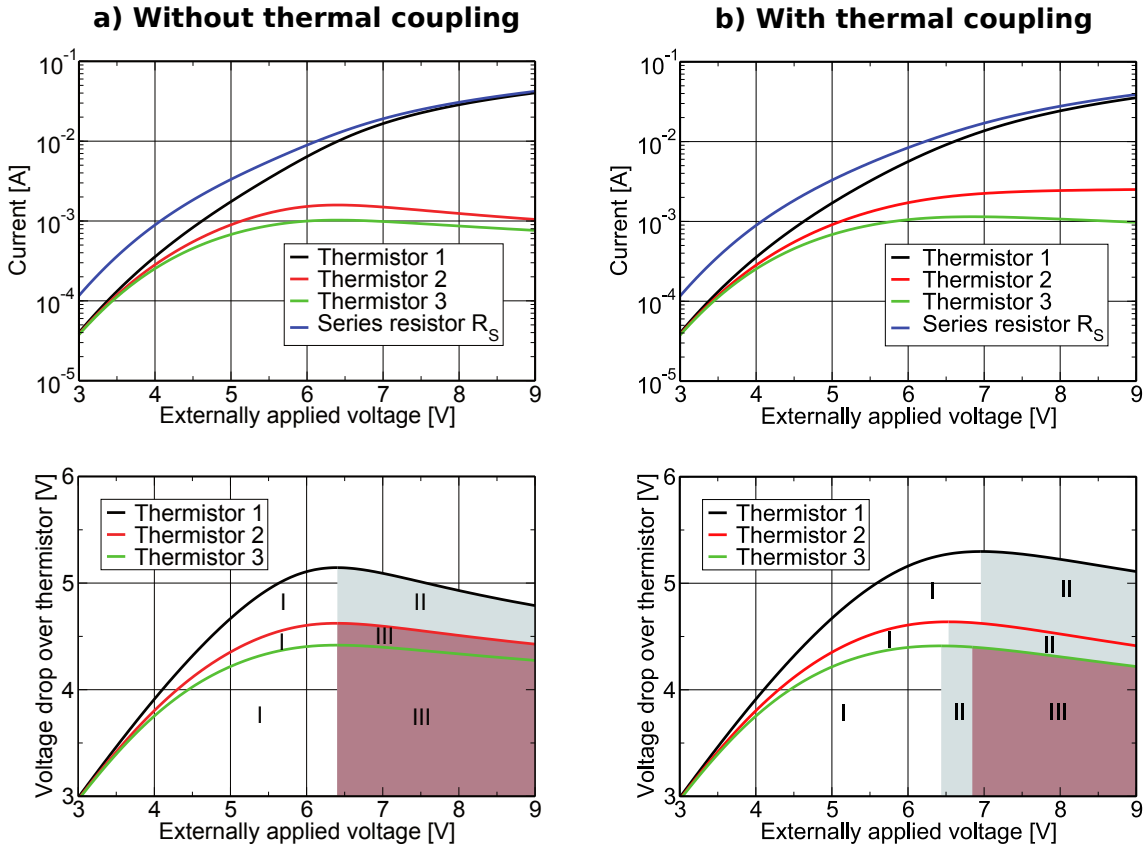

Figure 3: SPICE simulation of a 3-thermistor chain: Current (upper panels) and voltage (lower panels) of each single thermistor over the externally applied voltage V_{ext}. The left panels represent the situation without and the right panels with thermal coupling by a thermal resistance R_{coup} in Fig. 2 right.

voltage. The differential resistance of the other two thermistors remains positive at this critical voltage, though both $\frac{\mathrm{d}V_i}{\mathrm{d}V_{\mathrm{ext}}}$ and $\frac{\mathrm{d}I_i}{\mathrm{d}V_{\mathrm{ext}}}$ are negative, meaning that these thermistors are "switched off" by the first thermistor T_1.

In the thermally coupled case (b), for rising V_{ext} at first thermistor T_3 (green) shows S-NDR, then thermistor T_2 (red) follows for a slightly higher V_{ext}. If V_{ext} is increased further, T_3 (green) is switched back by T_2 (red) – goes to operation mode III. Finally, thermistor T_1 (black) switches to S-NDR. In other words, in the space resolved setting for rising V_{ext} the local NDR region moves from the right to the left in the device (see Fig. 2 left), and eventually the region furthest from the contact is switched back.

SPICE simulations for coupled electrical and thermal networks of an array of 10 times 10 thermistors have been successfully used in [11] to describe the behavior of OLEDs by evaluating currents and temperatures of each of the thermistors and by determining the different operation modes I, II and III in dependence of the applied voltage. Nevertheless, this network approach is geometrically inflexible and becomes inefficient for larger structures, and an adaptation of the mesh is problematic.

3   PDE model for large-area OLEDs

To obtain more freedom in the description of real geometrical device structures and to improve stability and speed of simulations, we propose a full PDE model for the electrothermal behavior of organic semiconductor structures. One of the main advantages of such a PDE system compared to the network model constructed in [11] is its flexibility with respect to variations of the device geometry and material composition. This property is crucial in simulation-based optimization of the device to reduce heat and current flow variations and to find device structures with lower sensitivity with respect to electrothermal feedback with the aim to reduce brightness inhomogeneities. In particular, the network model requires a careful construction of the network connections, which already in the uniform case becomes a challenging task. Moreover, parameters such as electric and thermal resistances depend on the network topology and have to be recalculated for new geometries. The algorithms used, e.g. in SPICE, to solve network models are not developed for large-scale problems with high aspect ratios and thus perform rather poorly. On the other hand, finite-element or finite-volume methods as well as mathematical tools in general for PDEs are well-established. There exists a variety of efficient numerical libraries and mesh generators, which allow for easy restructuring and simulation of the device. Additionally, a modeling based on PDEs can be used to systematically study stability and effects of symmetry breaking on pattern formation due to electrothermal feedback [23].

The derivation of the PDE system is guided by the electrothermal circuit model for OLED structures introduced in [11]. It is given by Kirchhoff's node and mesh rules and can be interpreted as a balancing of electrical and heat currents in a finite-volume discretized setting of a nonlinear PDE system with uniform cells, see Subsection 3.3.

The space resolved modeling we are proposing leads to a thermistor system consisting of a Laplace equation for the electrostatic potential φ coupled to the heat flow equation for the temperature distribution T. In particular, the electrical conductivity in the Laplace equation includes an Arrhenius-like temperature law and the non-Ohmic electric behavior

of the organic material. The heat flow equation contains the Joule heating as source term taking this special form of the electrical conductivity into account. This model also includes the contact resistance, an accurate spatially resolved translation of the Arrhenius-type current-voltage relation (2.1) for the active organic layer, and a local heat balance instead of the global one in (2.3). Note that in contrast to [25, 26], also the organic layer will be described by PDEs in our approach.

3.1 The PDE thermistor model

We start our modeling with the stationary situation by balancing the electric current density $\vec{j}$ and the density $\vec{q}$ of the heat flow,

$$\nabla \cdot \vec{j} = 0, \tag{3.1a}$$

$$\nabla \cdot \vec{q} = -(1 - \eta)\,\vec{j} \cdot \nabla \varphi. \tag{3.1b}$$

The modeling domain Ω consists of the organic device itself, the electrodes partly realized by the optically transparent but electrically not perfectly conducting ITO layer. In simulations it can be necessary to extend the domain in order to include the substrate glass or even the entire encapsulation for the heat balance equation.

With the additional introduction of the external power efficiency η for the generation of light in front of the Joule heating term in (3.1b), we take into account that a proportion of the electrical power is used for light out-coupling and does not produce heat ($\eta \approx 20\%$ in the active layer of an OLED, $\eta = 0$ in pure electronic devices). Dependencies of η on the temperature T and the flux $\vec{j}$ can also be included in the model. The constitutive relations between the flux densities and the gradients of the electric potential and the temperature, respectively, are given by

$$\vec{j} = -\sigma(x, T, |\nabla \varphi|)\nabla \varphi, \tag{3.2a}$$

$$\vec{q} = -\lambda(x)\nabla T. \tag{3.2b}$$

Here, σ and λ denote the electrical and thermal conductivity. For organic devices we have the non-Ohmic isothermal current-voltage relation (2.1) with $\alpha \neq 1$, which applies to OLEDs and other organic devices (comp. [13]). The electrical conductivity σ can in this case be expressed by

$$\sigma_{\text{org}}(T, |\nabla \varphi|) = \sigma_{\text{ref}}\Big[\frac{|\nabla \varphi|}{V_{\text{ref}}/d}\Big]^{\alpha - 1} F(T), \quad \sigma_{\text{ref}} = \frac{I_{\text{ref}}}{V_{\text{ref}}}\frac{d}{A},$$

where for normalization d and A denote the thickness and the area of the organic layer, respectively, and the function F is the Arrhenius-like conductivity factor given in (2.2). Therefore, the resulting current flow equation (3.1a) is of p-Laplacian type in the organic material, with $p = \alpha + 1$. For $\alpha > 1$ equation (3.1a) is of degenerated elliptic type in this subdomain. Subdomains without temperature-dependent conductivity, e.g. electrodes, are included by setting the activation energy $E_{\text{act}} = 0$ and introducing a spatially dependent function F. Moreover, to involve also Ohmic ($p = 2$) and non-Ohmic ($p > 2$) material

subdomains, we let p depend on the spatial position and formulate the following general expression for the electrical conductivity

$$\sigma(x, T, |\nabla\varphi|) = \sigma_0(x)\exp\Big[-\frac{E_{\mathrm{act}}(x)}{k_{\mathrm{B}}}\Big(\frac{1}{T}-\frac{1}{T_a}\Big)\Big]|\nabla\varphi|^{p(x)-2}. \tag{3.3}$$

According to the left panel of Fig. 2, the boundary conditions can be formulated as

$$\varphi = \varphi^+ \quad\text{on}\quad \Gamma_{V+}, \quad \varphi = \varphi^- \quad\text{on}\quad \Gamma_{V-}, \quad \vec{j}\cdot\nu = 0 \quad\text{on}\quad \Gamma_N, \tag{3.4a}$$

$$\vec{q}\cdot\nu = \kappa(x)(T-T_a) \quad\text{on}\quad \Gamma := \partial\Omega. \tag{3.4b}$$

The first two conditions in (3.4a) describe the current injection by prescribing the contact potentials φ_+ and φ_- at V_+ and V_-, respectively. On the part Γ_N, which does not belong to Γ_{V+} or Γ_{V-}, insulating boundary conditions are formulated. The Robin boundary conditions in (3.4b) for the heat flow equation express the heat transfer to the environment. The spatially dependent transfer coefficient κ takes care of the different surrounding materials. If one part of the boundary of the structure is cooled to ambient temperature (e.g. by a cooper block in experiments), the Dirichlet condition $T = T_a = \text{const}$ for the heat flow equation can be formulated on this part of the boundary.

The current-voltage relation for the entire device is obtained by

$$I(V_{\mathrm{ext}}) = \int_{\Gamma_{V+}} \sigma_{\mathrm{ITO}}\nabla\varphi\cdot\nu\,\mathrm{d}\Gamma. \tag{3.5}$$

Finally, let us mention that device structures with pure Ohmic behavior ($p = 2$) are included in our model. Such classical thermistor models have been investigated in the literature, e.g. [28] and Cimatti [4, 5] studied such models with different mixed boundary conditions using the Kohlrausch-Diesselhorst transformation.

3.2 A discretization scheme for the thermistor system

In this subsection we introduce a discretization scheme for (3.1)–(3.4), which is based on finite-volume methods, see e.g. [9]. In these methods the computational domain Ω is subdivided into a finite number of so-called Voronoi volumes K and the fluxes between two adjacent volumes are balanced. More precisely, the Voronoi decomposition of Ω consists of a family of nodes $x_i \in \overline{\Omega}$ and an associated family of control volumes K_i, which are constructed as follows: the set K_i is given as the set of all points in Ω whose Euclidean distance to x_i is not greater than their distance to all other sites x_j. The Voronoi volumes are convex, polygonal sets whose boundary faces are perpendicular to the line connecting two adjacent nodes of the mesh x_i and x_j, respectively. In particular, we can define a dual grid, consisting of triangles or tetrahedra in the two- or three-dimensional case, by connecting all pairwise adjacent nodes x_i. We assume that each triangle or tetrahedron of the dual grid belongs to only one material region (e.g. ITO or organic layer).

We aim to find a discrete analog of (3.1)–(3.2) for the quantities $T_i \approx T(x_i)$ and $\varphi_i \approx \varphi(x_i)$. In the following we will use the notation $\boldsymbol{\varphi} = \{\varphi_i\}$ and $\boldsymbol{T} = \{T_i\}$ to denote the families of nodal values.

For each Voronoi control volume K_i we integrate the current and heat flow equation over K_i and apply the Gauss theorem to the integral of the flux divergence to obtain

$$0 = \int_{K_i} \nabla \cdot \vec{j} \, dx = \sum_{S \in \mathcal{E}_{K_i}} \int_S \vec{j} \cdot \nu \, d\Gamma, \tag{3.6}$$

$$-\int_{K_i} (1-\eta)\vec{j} \cdot \nabla \varphi \, dx = \int_{K_i} \nabla \cdot \vec{q} \, dx = \sum_{S \in \mathcal{E}_{K_i}} \int_S \vec{q} \cdot \nu \, d\Gamma, \tag{3.7}$$

where $\mathcal{E}_{K_i}$ denotes the set of all boundary faces of K_i and ν denotes the unit normal vector to ∂K_i outward to K_i. In particular, if K_i shares parts of its boundary with $\partial\Omega$ the surface integrals can be replaced using the respective boundary condition: If on one of the faces S of K_i Dirichlet conditions are prescribed, i.e. $\varphi = \varphi^\pm$, we also fix $\varphi_i = \varphi^\pm$, while for homogeneous Neumann boundary conditions the respective surface integrals in (3.6) vanish. In the case of the Robin boundary conditions for the heat flux in (3.4) we have for $S \subset \partial K_i$ and $S \subset \partial\Omega$

$$\int_S \vec{q} \cdot \nu \, d\Gamma = \int_S \kappa(x)(T - T_a) \, d\Gamma \approx \kappa_S m_S (T_i - T_a), \tag{3.8}$$

where m_S denotes the measure of S and κ_S represents an approximation of κ on S.

To establish a discrete version of the current and heat flow equation in (3.1) we need to define suitable flux functions $g^\varphi_{i,S}(\boldsymbol{T}, \boldsymbol{\varphi})$ and $g^T_{i,S}(\boldsymbol{T})$, that approximate the current and heat fluxes from K_i into an adjacent volume K_j over the face S. Moreover, we have to find an approximation $Q_i(\boldsymbol{T}, \boldsymbol{\varphi})$ of the Joule heating term in the left-hand side of (3.7), integrated over K_i. With these notations, a finite-volume approximation may then be written in the form

$$\sum_{S \in \mathcal{E}_{K_i}} m_S g^\varphi_{i,S}(\boldsymbol{T}, \boldsymbol{\varphi}) = 0, \quad \text{and} \quad \sum_{S \in \mathcal{E}_{K_i}} m_S g^T_{i,S}(\boldsymbol{T}) = Q_i(\boldsymbol{T}, \boldsymbol{\varphi}). \tag{3.9}$$

In [3] a discretization scheme for the purely Ohmic case $p = 2$ was discussed. We follow the ideas and define for general p the flux functions for the current and heat flow by

$$g^\varphi_{i,S}(\boldsymbol{\varphi}, \boldsymbol{T}) = \begin{cases} \sigma_0 \, F(T_{ij}) A_S^{p-2} \frac{\varphi_i - \varphi_j}{|x_i - x_j|} & \text{in organic layer,} \\ \sigma_0 \frac{\varphi_i - \varphi_j}{|x_i - x_j|} & \text{otherwise,} \end{cases}$$
$$g^T_{i,S}(\boldsymbol{T}) = \lambda \frac{T_i - T_j}{|x_i - x_j|}. \tag{3.10}$$

Here, $T_{ij} = (T_i + T_j)/2$ is the arithmetic mean on S, and for faces S belonging to different material regions λ and σ_0 denote suitable averages of the conductivities. The crucial point is the quantity A_S, which is an approximation of the full norm of $\nabla\varphi$ and not only of the normal components. Our approach is the following: We denote by $\mathcal{T}_S$ the family of all triangles or tetrahedra $\omega \subset \Omega$ in the dual grid that share the edge $\overline{x_i x_j} \perp S$. On each ω the piecewise affine interpolant $\widehat{\varphi}$ with respect to the nodal values φ_i can be constructed, i.e. $\widehat{\varphi}$ is linear on each $\omega \in \mathcal{T}_S$ and $\widehat{\varphi}(x_i) = \varphi_i$. Now, A_S is defined to be the average of the norms of the respective gradients, namely

$$A_S = \sum_{\omega \in \mathcal{T}_S} \alpha_\omega |\nabla\widehat{\varphi}_{|\omega}| \quad \text{with} \quad \alpha_\omega = \frac{m_\omega}{\sum_{\widetilde{\omega} \in \mathcal{T}_S} m_{\widetilde{\omega}}}, \tag{3.11}$$

where m_ω denotes the measure of the set ω.

The approximation of the Joule term in the heat equation is not so straightforward since there is no natural discrete gradient defined on the control volumes – the approximate finite-volume solution is piecewise constant. Here, we basically follow the same lines as in [3], however, we include our extension for the non-Ohmic case and use the definition of A_S in (3.11). With d being the dimension of the computational domain we define

$$Q_i(\boldsymbol{T}, \boldsymbol{\varphi}) = (1-\eta)d \sum_{S \in \mathcal{E}_{K_i}} m_{D_{i,S}} \sigma_0 \, F(T_{ij}) A_S^{p-2} \Big(\frac{\varphi_i - \varphi_j}{|x_i - x_j|} \Big)^2, \tag{3.12}$$

where for the control volume K_i and $S \in \mathcal{E}_{K_i}$ we define the half-diamond $D_{i,S}$ as the convex hull of x_i and S, i.e.

$$D_{i,S} = \big\{ \theta x_i + (1-\theta)x : (\theta, x) \in (0,1) \times S \big\} \quad \text{such that} \quad \overline{K_i} = \bigcup_{S \in \mathcal{E}_{K_i}} \overline{D}_{i,S}.$$

Note that a face S of a control volume can in general belong to different materials. In this case one can split the flux over the edge additively and replace the factor m_S in (3.9) by the length (or area) of the face in the respective material (see discussion in Section 3.3.2). The same applies for the Joule heating term in (3.12). In practice, this is easily done since the assembly of the discrete system is done triangle- or tetrahedron-wise.

Remark 3.1 *Using a finite-volume based formulation of the thermistor model the appearance of local negative differential resistance can be investigated as follows: On the grid between neighboring cells K_i and K_j the differential resistance is given by*

$$\frac{dV_{ij}}{dI_{ij}} = \frac{\partial(\varphi_j - \varphi_i)}{\partial V_{\text{ext}}} \Big(\frac{\partial I_{ij}}{\partial V_{\text{ext}}} \Big)^{-1}, \tag{3.13}$$

where I_{ij} is the inter-volume current and V_{ext} represents the total applied voltage. Therefore the position of these regions in dependence on the total current or total applied voltage can be detected. Thus the presented scheme allows us to study the appearance of spatially local NDR regions and the propagation of NDR fronts through the OLED device in dependence on the total current by self-consistent electrothermal simulations.

3.3   The relation between PDE and network model

In this subsection we establish the connection between the system of partial differential equations in (3.1) and the thermistor network discussed in [11]. More precisely, we show that the Kirchhoff circuit laws for the electric network can be interpreted as a finite-volume discretization with additional assumptions on the device geometry.

For notational simplicity we restrict ourselves to the two-dimensional case depicted in Fig. 2 left. In particular, we assume that the cross-section of the relevant regions of the OLED, comprising of the ITO and the organic layer, can be described by rectangular subdomains. More precisely, the two layers are given by $\Omega_{\text{ITO}} = (0,L) \times (0,h_1)$ and $\Omega_{\text{org}} = (0,L) \times (h_1, h_2)$. Note that we have flipped the device structure upside down

compared to Fig. 2 left. Typically, the thickness of each layer is about 100 nm, hence we set $h_1 = h$, $h_2 = 2h$. The length L is in the milli- to centimeter range such that $h/L \ll 1$ is satisfied.

The device is contacted on the metal layer. However, due to the high conductivity of this layer we can assume that the potential in the metal layer is constant. In particular, we neglect the metal layer entirely by prescribing Dirichlet boundary conditions on the top of the organic layer, i.e. $\varphi = \varphi^-$ on $(0, L) \times \{2h\}$. The second contact is applied at right end of the ITO layer and we set $\varphi = \varphi^+$ on $\{L\} \times (0, h)$. On the remaining boundary no-flux boundary conditions are assumed.

Finally, the temperature distribution is computed on an extended domain that includes the glass substrate (or possibly the entire encapsulation of the device). Boundary conditions of third type model the heat conduction into the environment (e.g. air or a copper block).

3.3.1   The thermistor network model

We briefly describe the network model established in [11]. As in Fig. 2 the network is comprised of two sub-networks: an electrical and a thermal network. The latter accounts for the heat flow with the electrical power dissipation in the electrical part acting as heat source. In the thermal network, a resistor corresponds to a thermal resistance, a voltage represents a temperature difference, and a current represents a heat flow.

The organic layer is represented by an array of thermistor devices such that the current flowing in each thermistor (given by relation (2.1)) equals the vertical current flow through a certain volume part of the organic layer. Lateral electric conductance of the organic layer is neglected due to much larger conductivity of the ITO. Moreover, each thermistor is coupled to a thermal network by the dissipation of power. Thus, following [17] each thermistor is modeled as a three terminal device. The ITO layer (anode) is modeled by connecting all lower electrical contacts of the thermistor array via a network of resistors. Hence, each thermistor is connected to its nearest neighbors by a resistor representing the sheet resistance. For simplicity, it is assumed that the metal layer (cathode) has a much lower resistivity than the ITO layer such that its influence can be neglected. Thus, all upper cathode contacts of the thermistor array are directly connected to each other. Finally, the electric grid is connected to the power supply with the voltage $V+$ via resistors.

For simplicity, the thermal network only models the heat flow in the glass substrate and the heat transport into the environment, i.e. horizontal heat flow in the thin electrical active regions is neglected. Besides heat generated by the thermistor devices, Ohmic losses along the ITO are also fed into the thermal network.

3.3.2   From the PDE to the network model via finite-volume discretization

The passage from the PDE model (3.1)–(3.4) to the discrete network model described in the previous section is realized by introducing a family of suitable control volumes K. Here, we use the same geometry as in Fig. 2 left and we assume additionally that the length of the active region is a multiple of the thickness of the organic layer, i.e. $L = Nh$
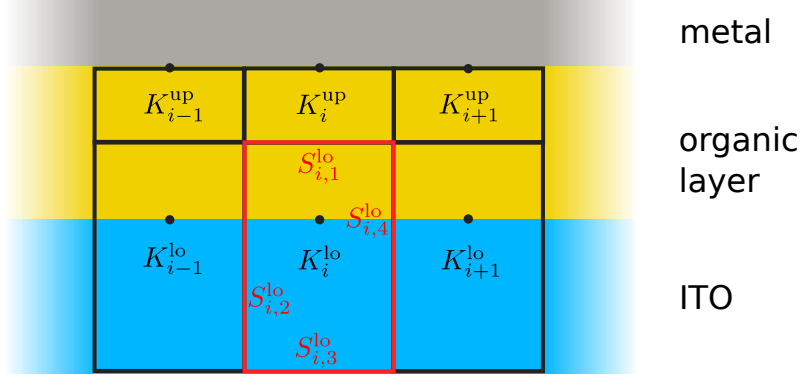
Figure 4: Control volumes used for passage to discrete network model (structure is turned upside down compared to Fig. 2 left).

with $N \in \mathbb{N}$. Due to its high conductivity we can replace the metal layer by setting Dirichlet conditions on the top of the organic layer.

We define control volumes by introducing the families of upper and lower nodes $x_i^{\text{up}} = (ih, 2h)$ and $x_i^{\text{lo}} = (ih, h)$ for $i = 0, \ldots, N$. With this, the control volumes $K_i^{\text{up}}, K_i^{\text{lo}} \subset \Omega$ are given as the Voronoi boxes associated with the nodes x_i^{up} and x_i^{lo}. In particular, the edge shared by K_i^{up} and K_i^{lo} lies in the center of the organic layer while the edge between $K_i^{\text{up/lo}}$ and $K_{i+1}^{\text{up/lo}}$ is located in the fiber $\{(i+1/2)h\} \times \mathbb{R}$. For $i = 1, \ldots, N-1$ the length of each volume $K_i^{\text{up/lo}}$ is given by h, while $K_0^{\text{up/lo}}$ and $K_N^{\text{up/lo}}$ are only $h/2$ long.

We denote by $S_{i,1}^{\text{up/lo}}$, $S_{i,2}^{\text{up/lo}}$, $S_{i,3}^{\text{up/lo}}$, and $S_{i,4}^{\text{up/lo}}$ the top, left, bottom, and right face of a Voronoi volume $K_i^{\text{up/lo}}$, respectively (see Fig. 4).

We can now apply the discretization scheme developed in Section 3.2. In particular, since we have prescribed Dirichlet conditions on the top of the organic layer and on the right side of the ITO we set $\varphi_i^{\text{up}} = \varphi^-$ for $i = 0, \ldots, N$ and $\varphi_N^{\text{lo}} = \varphi^+$, respectively. Moreover, due to the homogeneous Neumann boundary conditions on the remaining boundary there are no fluxes through $S_{i,3}^{\text{lo}}$ for $i = 0, \ldots, N-1$, $S_{0,2}^{\text{up/lo}}$, and $S_{N,4}^{\text{up}}$.

First, we consider only the flux through the upper face $S_{i,1}^{\text{lo}}$, for $i = 0, \ldots, N-1$, i.e. in the organic layer. With the definition of the flux function in (3.10) the total flux through $S_{i,1}$ is given by $\sigma_{\text{org}} F(T_i^{\text{mi}}) A_{S_{i,1}}^{p-2} (\varphi^- - \varphi_i^{\text{lo}})$, where $T_i^{\text{mi}} = (T_i^{\text{up}} + T_i^{\text{lo}})/2$ denotes the average temperature. Assuming that the lateral differences $\varphi_{i+1}^{\text{lo}} - \varphi_i^{\text{lo}}$ are small compared to the vertical differences $\varphi^- - \varphi_i^{\text{lo}}$ we can replace $A_{S_{i,1}}$ by $|\varphi^- - \varphi_i^{\text{lo}}|$. Hence, by defining the local voltage drop across $S_{i,1}^{\text{lo}}$ by $U_i = \varphi_i^{\text{lo}} - \varphi^-$ we have found that the vertical current into the node x_i^{lo} is given by

$$j_{\text{vert},i} = \sigma_{\text{org}} F(T_i^{\text{mi}}) |U_i|^{p-2} U_i.$$

Next, we look at the current flow through the left or right face. The above assumption yields that lateral currents in the organic layers can be neglected (comp. [25, 26]). Hence, the current flow through $S_{i,2}^{\text{lo}}$ and $S_{i,4}^{\text{lo}}$ into the node x_i^{lo} is given by $j_{\text{lat},i-} = \sigma_{\text{ITO}}(\varphi_{i-1}^{\text{lo}} - \varphi_i^{\text{lo}})$ and $j_{\text{lat},i+} = \sigma_{\text{ITO}}(\varphi_{i+1}^{\text{lo}} - \varphi_i^{\text{lo}})$, respectively.

Thus, the finite-volume discretization reproduces Kirchhoff's nodal law for the thermistor network of [11]

$$0 = j_{\text{vert},i} + j_{\text{lat},i+} + j_{\text{lat},i-}.$$

The computation of the Joule sources via (3.12) is straight-forward. In particular, the power dissipated in the entire column $K_i^{\text{up}} \cup K_i^{\text{lo}}$ is given by

$$Q_i = (1-\eta)\sigma_{\text{org}}F(T_i^{\text{mid}})U_i^p + \frac{\sigma_{\text{ITO}}}{2}\big((\varphi_i^{\text{lo}} - \varphi_{i-1}^{\text{lo}})^2 + (\varphi_{i+1}^{\text{lo}} - \varphi_i^{\text{lo}})^2\big).$$

The derivation of the thermal network is analogously. Note however that [11] makes simplifying assumptions on the temperature distribution. Namely, heat flow in the electric active region can be neglected and the Joule heating acts as line source on the top of the glass substrate.

It is easy to see that the above procedure can be extended to the three dimensional case, where the rectangular control volumes $K_i^{\text{up/lo}}$ are replaced by cuboids with length and depth h, respectively.

4   Mathematical analysis for the *p*-Laplace thermistor model

In this section we consider the special case of the equations (3.1) – (3.4) with spatially constant exponent $p > 2$. Then our problem reads as

$$-\nabla \cdot \big(\sigma_0(x)F(x,T)|\nabla\varphi|^{p-2}\nabla\varphi\big) = 0 \quad \text{on} \quad \Omega, \tag{4.1a}$$

$$-\nabla \cdot (\lambda(x)\nabla T) = (1-\eta)\sigma_0(x)F(x,T)|\nabla\varphi|^p \quad \text{on} \quad \Omega \tag{4.1b}$$

together with the mixed boundary conditions

$$\varphi = \varphi^D \quad \text{on} \quad \Gamma_D, \quad -\sigma_0(x)F(x,T)|\nabla\varphi|^{p-2}\nabla\varphi \cdot \nu = 0 \quad \text{on} \quad \Gamma_N, \tag{4.2a}$$

$$-\lambda(x)\nabla T \cdot \nu = \kappa(x)(T - T_a) \quad \text{on} \quad \Gamma, \tag{4.2b}$$

where φ^D is a function representing the Dirichlet values at all electrical contacts.

We are going to prove the existence of weak solutions to the problem (4.1)–(4.2) using Schauder's fixed-point theorem for the temperature distribution T, see Theorem 4.2. First for a given temperature distribution $\widetilde{T}$ we obtain a unique solution $\varphi(\widetilde{T})$ of the current flow equation (4.1a) and prove L^∞-bounds and regularity results for $\varphi(\widetilde{T})$ (Lemma 4.1 and Lemma 4.2). Next, exploiting these regularity results we give a weak formulation for the coupled problem and establish a priori estimates for the solution (Theorem 4.1). Finally, we show that this solution can be obtained via a fixed-point map $T = Q(\widetilde{T})$, where T solves the heat equation (4.1b) for the Joule heat given by the electrostatic potential $\varphi(\widetilde{T})$ and $F(\widetilde{T})$.

4.1   Assumptions and preliminaries

For the analytical investigations we make the following assumptions on the domain, boundary data, and coefficients introduced in Subsection 3.1:

(A) $\Omega \subset \mathbb{R}^2$ bounded Lipschitzian domain, Γ_D, Γ_N are disjoint open subsets of
$\Gamma := \partial\Omega$, $\mathrm{mes}\,\Gamma_D > 0$, $\Gamma = \Gamma_D \cup \Gamma_N \cup (\overline{\Gamma_D} \cap \overline{\Gamma_N})$, $\overline{\Gamma_D} \cap \overline{\Gamma_N}$ consists of finitely
many points ($\Omega \cup \Gamma_N$ is regular in the sense of Gröger [15]),
$p > 2$, $\varphi^D \in W^{1,\infty}(\Omega)$, $\sigma : \Omega \times \mathbb{R}_+ \times \mathbb{R}_+ \to \mathbb{R}$, $\sigma(x, T, z) = \sigma_0(x) F(T) z^{p-2}$,
σ_0, $\lambda \in L^\infty(\Omega)$, $0 < \underline{\sigma_0} \le \sigma_0 \le \overline{\sigma_0}$, $\lambda \ge c > 0$ a.e. on Ω,
$F(x, T) = \exp\Big[-\beta(x)\Big(\frac{1}{T} - \frac{1}{T_a}\Big)\Big]$, $\beta \in L^\infty_+(\Omega)$,
$T_a \in \mathbb{R}$, $T_a > 0$, $\eta = \eta(x, T, j)$, $\eta : \Omega \times \mathbb{R} \times \mathbb{R}^2 \to \mathbb{R}$ Caratheodory function,
$\eta \in [0, 1]$ a.e. in Ω, $\forall (T, j) \in \mathbb{R} \times \mathbb{R}^2$, $\kappa \in L^\infty_+(\Gamma)$, $\|\kappa\|_{L^1(\Gamma)} > 0$.

For $p \in (1, \infty)$ we work with the Sobolev spaces

$$W^{1,p}(\Omega) = \{u \in L^p(\Omega) : D^\alpha u \in L^p(\Omega) \text{ for } |\alpha| \le 1\}$$

equipped with the norm

$$\|u\|_{W^{1,p}}^p = \sum_{|\alpha| \le 1} \|D^\alpha u\|_{L^p}^p$$

and

$$W_0^{1,p}(\Omega \cup \Gamma_N) = \{u \in W^{1,p}(\Omega) : u|_{\Gamma_D} = 0\}.$$

For $p = 2$ we also write $H^1(\Omega)$ instead of $W^{1,2}(\Omega)$. Moreover, the dual space of a Banach space X is denoted by X^*.

For the treatment of the p-Laplace expressions we make use of the following inequalities: Due to convexity of the function $y \mapsto |y|^p$ for $p \ge 1$, the inequality

$$\left|\frac{y+z}{2}\right|^p \le \frac{|y|^p + |z|^p}{2} \quad \text{for} \quad y, z \in \mathbb{R}^n \tag{4.3}$$

is fulfilled. Exploiting the subdifferential estimate we have the inequality

$$|y|^p \ge |z|^p + p|z|^{p-2} z \cdot (y - z) \quad \text{if } p \ge 1, \quad y, z \in \mathbb{R}^n. \tag{4.4}$$

Additionally, we apply the inequality

$$\begin{aligned}
\langle |y|^{p-2} y - |z|^{p-2} z, y - z\rangle &\ge 2^{-1}(|y|^{p-2} + |z|^{p-2})|y - z|^2 \\
&\ge 2^{2-p}|y - z|^p \quad \text{if } p \ge 2, \quad y, z \in \mathbb{R}^n,
\end{aligned} \tag{4.5}$$

which can be found in [19, Chapter 10].

4.2   Properties of the current flow equation

We introduce the set of relevant temperature distributions $\mathcal{T}$ via

$$\mathcal{T} = \{T \in H^1(\Omega) \cap L^\infty(\Omega) : T \ge T_a \text{ a.e. on } \Omega\}. \tag{4.6}$$

According to (A) for $T \in \mathcal{T}$ we find

$$\sigma_0 F(\cdot, T) \in L^\infty(\Omega) \quad \text{and} \quad \sigma_0 F(\cdot, T) \in [\underline{\sigma_0}, \overline{\sigma_0}\, \mathrm{e}^{\|\beta\|_{L^\infty}/T_a}) =: [\sigma_1, \sigma_2). \qquad (4.7)$$

For a fixed function $T \in \mathcal{T}$ we define the nonlinear operator $A_T : \varphi^D + W_0^{1,p}(\Omega \cup \Gamma_N) \to (W_0^{1,p}(\Omega \cup \Gamma_N))^*$ by

$$\langle A_T(\varphi), v \rangle := \int_\Omega \sigma(x, T, |\nabla\varphi|)\nabla\varphi \cdot \nabla v \,\mathrm{d}x, \quad v \in W_0^{1,p}(\Omega \cup \Gamma_N),$$

and consider the following problem: Find an electrostatic potential $\varphi \in \varphi^D + W_0^{1,p}(\Omega \cup \Gamma_N)$ such that

$$\langle A_T(\varphi), v \rangle = 0 \quad \text{for all } v \in W_0^{1,p}(\Omega \cup \Gamma_N), \qquad (4.8)$$

which corresponds to a weak solution $\varphi \in \varphi^D + W_0^{1,p}(\Omega \cup \Gamma_N)$ of the p-Laplace-type equation (4.1a) with boundary conditions (4.2a) for the given temperature distribution T.

Lemma 4.1 *We assume (A). Let $T \in \mathcal{T}$ be a fixed given function. Then equation (4.8) has exactly one solution φ. Moreover, there are constants $c_\varphi > 0$ and $c_\infty > 0$ independent of the chosen T, depending only on the data (Ω, φ^D, $\underline{\sigma_0}$, $\overline{\sigma_0}$, T_a, and β) such that*

$$\|\varphi\|_{W^{1,p}} \le c_\varphi, \quad \max_{x \in \overline{\Omega}} |\varphi(x)| \le c_\infty.$$

Proof. Let $h^+ = \max(h, 0)$, $h^- = \max(-h, 0)$ denote the positive and negative part of a function h, respectively.

1. First, we show the bounds of solutions to (4.8). Let $\overline{\varphi^D} := \|\varphi^D\|_{L^\infty}$ and $\underline{\varphi^D} :=$ ess $\inf_{x \in \Omega} \varphi^D$. Then the test of (4.8) by $(\varphi - \overline{\varphi^D})^+ \in W_0^{1,p}(\Omega \cup \Gamma_N)$ gives

$$0 = \int_\Omega \sigma(\cdot, T, |\nabla\varphi|)|\nabla(\varphi - \overline{\varphi^D})^+|^2 \,\mathrm{d}x \ge \int_\Omega \sigma_1 |\nabla(\varphi - \overline{\varphi^D})^+|^p \,\mathrm{d}x$$

leading to $\varphi \le \overline{\varphi^D}$ a.e. in Ω. On the other hand, the test of (4.8) by $-(\varphi - \underline{\varphi^D})^-$ ensures

$$0 = \int_\Omega \sigma(\cdot, T, |\nabla\varphi|)|\nabla(\varphi - \underline{\varphi^D})^-|^2 \,\mathrm{d}x \ge \int_\Omega \sigma_1 |\nabla(\varphi - \underline{\varphi^D})^-|^p \,\mathrm{d}x$$

and therefore $\varphi \ge \underline{\varphi^D}$ a.e. in Ω.

To obtain the $W^{1,p}$-estimate, we use the test function $\varphi - \varphi^D$ for (4.8)

$$\int_\Omega \sigma_1 |\nabla\varphi|^p \,\mathrm{d}x \le \int_\Omega \sigma_2 |\nabla\varphi|^{p-1}|\nabla\varphi^D| \,\mathrm{d}x \le \int_\Omega \left\{ \frac{\sigma_2}{2} |\nabla\varphi|^p + c|\nabla\varphi^D|^p \right\} \mathrm{d}x$$

which together with the L^∞-bounds of φ leads to $\|\varphi\|_{W^{1,p}} \le c$. Since $p > 2$, the solution φ is continuous and the upper and lower bounds hold true for all $x \in \Omega$.

2. The operator A_T is monotone and continuous. By (4.5) we obtain

$$\langle A_T\varphi, \varphi - \varphi^D \rangle \ge \int_\Omega \left\{ \sigma_0 F(\cdot, T) 2^{2-p} |\nabla(\varphi - \varphi^D)|^p - \sigma_2 |\nabla\varphi^D|^{p-1}|\nabla(\varphi - \varphi^D)| \right\} \mathrm{d}x$$

$$\ge c\|\nabla(\varphi - \varphi^D)\|_{L^p}^p - c_1 \|\nabla(\varphi - \varphi^D)\|_{L^p} \|\nabla\varphi^D\|_{L^p}^{p-1}.$$

Since $|\Gamma_D| > 0$, the norm $\|\nabla \cdot\|_{L^p}$ is an equivalent norm in $W_0^{1,p}(\Omega \cup \Gamma_N)$, and the previous inequality ensures together with $\varphi^D \in W^{1,\infty}(\Omega)$ the coercivity of the operator A_T. Therefore the main theorem of monotone operators (see [14, 30]) guarantees the existence of a solution to (4.8). Equation (4.8) is the weak Euler-Lagrange equation associated with the minimization problem

$$\min_{\varphi \in \varphi^D + W_0^{1,p}(\Omega \cup \Gamma_N)} \int_\Omega G(x, \nabla\varphi) \, \mathrm{d}x, \quad G(x, \nabla\varphi) := \frac{\sigma_0(x)F(x, T(x))}{p}|\nabla\varphi|^p. \tag{4.9}$$

To see this, we show first '(4.9) $\Rightarrow$ (4.8)': If φ is a minimizer, we consider $\varphi + \epsilon v$, where $v \in W_0^{1,p}(\Omega \cup \Gamma_N)$ and ϵ is a real parameter. Since $J(\epsilon) := \int_\Omega G(x, \nabla(\varphi + \epsilon v)) \, \mathrm{d}x$ takes its minimum at $\epsilon = 0$ and $\epsilon \mapsto J(\epsilon)$ is differentiable we have $J'(0) = 0$ which corresponds to (4.8). Next we show '(4.8) $\Rightarrow$ (4.9)'. Due to convexity we have for $p \geq 2$ the inequality (4.4), which ensures for all $v \in W_0^{1,p}(\Omega \cup \Gamma_N)$ that

$$\int_\Omega \frac{\sigma_0 F(\cdot, T)}{p}|\nabla(\varphi + v)|^p \, \mathrm{d}x \geq \int_\Omega \frac{\sigma_0 F(\cdot, T)}{p}|\nabla\varphi|^p \, \mathrm{d}x$$
$$+ \int_\Omega \sigma_0 F(\cdot, T)|\nabla\varphi|^{p-2}\nabla\varphi \cdot \nabla v \, \mathrm{d}x.$$

If (4.8) is fulfilled then the last integral vanishes and we obtain (4.9).

Next, we suppose there would be two different solutions φ^1 and φ^2 to the minimum problem (4.9). If $\nabla\varphi^1 \neq \nabla\varphi^2$ on a set of positive measure, the inequality (4.3) is strict on this set which leads to

$$\int_\Omega \frac{\sigma_0 F(\cdot, T)}{p}|\nabla\varphi^1|^p \, \mathrm{d}x \leq \int_\Omega \frac{\sigma_0 F(\cdot, T)}{p}\Big|\nabla\Big(\frac{\varphi^1 + \varphi^2}{2}\Big)\Big|^p \, \mathrm{d}x$$
$$< \frac{1}{2}\int_\Omega \frac{\sigma_0 F(\cdot, T)}{p}\Big\{|\nabla\varphi^1|^p + |\nabla\varphi^2|^p\Big\} \, \mathrm{d}x$$
$$= \int_\Omega \frac{\sigma_0 F(\cdot, T)}{p}|\nabla\varphi^1|^p \, \mathrm{d}x$$

which gives a contradiction. Therefore, $\nabla\varphi^1 = \nabla\varphi^2$ holds a.e. in Ω. Since $\varphi^1 - \varphi^2 \in W_0^{1,p}(\Omega \cup \Gamma_N)$ this proves the uniqueness of the solution to (4.9) as well as (4.8). $\square$

The next aim is to show higher regularity of this weak solution, namely $\varphi \in W^{1,ps^*}(\Omega)$, with a uniform $s^* > 1$ for all arbitrarily given $T \in \mathcal{T}$.

Lemma 4.2 *We assume (A). Then there exist constants $p^* = ps^* > p$ and $c_{p^*} > 0$ depending only on the data (Ω, φ^D, $\underline{\sigma_0}$, $\overline{\sigma_0}$, T_a, and β) such that the solution φ to (4.8) belongs to $W^{1,p^*}(\Omega)$ with $\|\varphi\|_{W^{1,p^*}} \leq c_{p^*}$ uniformly for all given functions $T \in \mathcal{T}$.*

Proof. We intend to apply Theorem 3.1 in [10] and have to verify the needed assumptions (A1), (A2) and (A3) for this theorem. Our spatial setting fits to (A1). The function $H : \Omega \times \mathbb{R}^2 \to \mathbb{R}$ defined by

$$H(x, \xi) := \frac{\sigma_0(x)F(x, T(x))}{p}|\xi + \nabla\varphi^D|^p$$

is a Caratheodory function. Using (4.7) and exploiting that $\varphi^D \in W^{1,\infty}(\Omega)$ we can estimate

$$|H(x,\xi)| \leq \frac{\sigma_2}{p}(|\xi| + \vartheta(x))^p \quad \text{f.a.a. } x \in \Omega, \quad \forall \xi \in \mathbb{R}^2$$

with $\vartheta(x)^p := r \, |\nabla\varphi^D|^p \in L^1(\Omega)$, where $r := \max\{1, \frac{\sigma_1}{p}\}$, $\vartheta^p \geq 0$, which yields (A2).

Defining the function $\widetilde{H} : \mathbb{R}^2 \to \mathbb{R}$ by $\widetilde{H}(\xi) = 2^{1-p}\frac{\sigma_1}{p}|\xi|^p$ we have $\widetilde{H}(0) = 0$ and for all $\varphi_0 \in W_0^{1,p}(\Omega \cup \Gamma_N)$ there holds

$$\int_\Omega \widetilde{H}(\nabla\varphi_0) \, \mathrm{d}x \geq 2^{1-p}\frac{\sigma_1}{p}\|\nabla\varphi_0\|_{L^p}^p.$$

Additionally, for a.a. $x \in \Omega$ and all $\xi \in \mathbb{R}^2$ the lower estimate

$$H(x,\xi) \geq \frac{\sigma_1}{p}|\xi + \nabla\varphi^D|^p \geq \frac{\sigma_1}{p}\left[2\left|\frac{\xi}{2}\right|^p - |\nabla\varphi^D|^p\right]$$

$$= 2^{1-p}\frac{\sigma_1}{p}|\xi|^p - \frac{\sigma_1}{p}|\nabla\varphi^D|^p \geq \widetilde{H}(\xi) - \vartheta(x)^p$$

is valid. Here we used inequality (4.3) with $z = \xi + \nabla\varphi^D$ and $y = \nabla\varphi^D$. Thus, also (A3) is verified. To conclude, the assumptions (A1), (A2) and (A3) needed in Theorem 3.1 in [10] are fulfilled. Thus, this theorem guarantees the existence of $s^* > 1$ such that for $p > 2$

$$\int_\Omega |\nabla(\varphi - \varphi^D)|^{ps^*} \, \mathrm{d}x \leq c\left\{\left(\int_\Omega |\nabla(\varphi - \varphi^D)|^p \, \mathrm{d}x\right)^{s^*} + \int_\Omega (\theta(x)^p + 1)^{s^*} \, \mathrm{d}x\right\}, \qquad (4.10)$$

see (3.4) in [10]. Note that the right hand side in (4.10) is bounded by constants depending only on the data. Due to the L^∞-bounds of φ, φ^D, and $|\nabla\varphi^D|$ we find that $\|\varphi\|_{W^{1,p^*}} \leq c_{p^*}$ uniformly for all given functions $T \in \mathcal{T}$.   □

Corollary 4.1 *We assume (A). Then for the exponent $s^* > 1$ from Lemma 4.2 there exists a constant $c_{s^*} > 0$ depending only on the data (Ω, φ^D, $\underline{\sigma_0}$, $\overline{\sigma_0}$, T_a, and β) such that for all given functions $T \in \mathcal{T}$ the solution φ to (4.8) fulfills the estimate*

$$\|(1 - \eta)\sigma_0 F(\cdot, T)|\nabla\varphi|^p\|_{L^{s^*}} \leq c_{s^*}.$$

Proof. According to Lemma 4.2 we know that $\|\varphi\|_{W^{1,ps^*}} \leq c_{p^*}$ which together with Assumption (A) and (4.7) ensures that the expression $(1 - \eta)\sigma(x, T, \nabla\varphi)|\nabla\varphi|^2$ belongs to $L^{s^*}(\Omega)$ and the norm can be estimated by

$$\|(1 - \eta)\sigma_0 F(\cdot, T)|\nabla\varphi|^p\|_{L^{s^*}} \leq \sigma_2\||\nabla\varphi|^p\|_{L^{s^*}} \leq \sigma_2\||\nabla\varphi|\|_{L^{ps^*}}^p \leq c_{s^*}.   □$$

4.3   The coupled thermistor problem

To tackle the full problem, we introduce the nonlinear operator $A : (\varphi^D + W_0^{1,p^*}(\Omega \cup \Gamma_N)) \times (H^1(\Omega) \cap L^\infty(\Omega)) \to (W_0^{1,p}(\Omega \cup \Gamma_N))^* \times H^1(\Omega)^*$ by

$$\langle A(\varphi, T), (\overline{\varphi}, \overline{T})\rangle := \int_\Omega \sigma(x, T, |\nabla\varphi|)\nabla\varphi \cdot \nabla\overline{\varphi} + \lambda(x)\nabla T \cdot \nabla\overline{T} \, \mathrm{d}x$$

$$- \int_\Omega (1 - \eta(j, T))\sigma(x, T, |\nabla\varphi|)|\nabla\varphi|^2\overline{T} \, \mathrm{d}x \qquad (4.11)$$

$$+ \int_\Gamma \kappa(T - T_a)\overline{T} \, \mathrm{d}\Gamma \qquad \forall\overline{\varphi} \in W_0^{1,p}(\Omega \cup \Gamma_N), \forall\overline{T} \in H^1(\Omega)$$

and look for solutions to Problem (P)

$$A(\varphi, T) = 0, \quad \varphi \in \varphi^D + W_0^{1,p^*}(\Omega \cup \Gamma_N), \quad T \in H^1(\Omega) \cap L^\infty(\Omega) \tag{P}$$

which correspond to the weak solutions to the system (4.1a) – (4.2b).

Theorem 4.1 (Bounds) *We assume (A). Then there exist constants c_{p^*}, c_{q^*}, $c_\infty > 0$ and an exponent $q^* > 2$ such that any weak solution (φ, T) to Problem (P) fulfills*

$$\|\varphi\|_{W^{1,p^*}} \le c_{p^*}, \quad \max_{x \in \overline{\Omega}} |\varphi(x)| \le c_\infty,$$

$$\|T\|_{W^{1,q^*}} \le c_{q^*}, \quad T_a \le T(x) \le c_\infty \quad \text{for all } x \in \Omega.$$

Proof. 1. For the lower bound of the temperature distribution we test Problem (P) by $-(0, (T - T_a)^-)$ and obtain

$$\int_\Omega \lambda |\nabla (T - T_a)^-|^2 \, \mathrm{d}x + \int_\Gamma \kappa ((T - T_a)^-)^2 \, \mathrm{d}\Gamma \le 0$$

which ensures that $T \ge T_a$ a.e. in Ω.

2. If (φ, T) is a solution to (P) then φ solves (4.8) for this T and the estimates for the component φ of the solution result from Lemma 4.1 and Lemma 4.2.

3. By Corollary 4.1 we know that the Joule heating term in the right hand side of the heat equation, $(1 - \eta)\sigma(x, T, \nabla\varphi)|\nabla\varphi|^2$, belongs to $L^{s^*}(\Omega)$ and its L^{s^*}-norm can be estimated by c_{s^*}. We use regularity results for second order elliptic equations with nonsmooth data in the two-dimensional case (see [15]). According to [15, Theorem 1] there is a $\widetilde{q} > 2$ such that the strongly monotone Lipschitz continuous operator $\widetilde{B} : H^1(\Omega) \to H^1(\Omega)^*$,

$$\langle \widetilde{B}T, w \rangle := \int_\Omega (\lambda \nabla T \cdot \nabla w + Tw) \, \mathrm{d}x, \quad w \in H^1(\Omega),$$

maps $W^{1,q}(\Omega)$ into and onto $W^{-1,q}(\Omega)$ for all $q \in [2, \widetilde{q}]$. Here $W^{-1,q}(\Omega)$ means $W^{1,q'}(\Omega)^*$, where $\frac{1}{q} + \frac{1}{q'} = 1$. Next we define $q^* \in (2, \widetilde{q}]$ by

$$q^* := \begin{cases} \widetilde{q} & \text{if } \dfrac{s^*}{s^* - 1} \in \left[1, \dfrac{2\widetilde{q}}{\widetilde{q} - 2}\right] \\ \dfrac{2s^*}{2 - s^*} & \text{if } \dfrac{s^*}{s^* - 1} > \dfrac{2\widetilde{q}}{\widetilde{q} - 2} \end{cases}, \qquad \frac{1}{q^*} + \frac{1}{(q^*)'} = 1.$$

This definition guarantees that $L^{s^*}(\Omega) \hookrightarrow W^{-1,q^*}(\Omega) = W^{1,(q^*)'}(\Omega)^*$. Remark 13 in [15] then ensures W^{1,q^*} estimates for solutions to problems $\widetilde{B}T = R(T)$, where R is any mapping from $W^{1,2}(\Omega)$ into $W^{-1,q^*}(\Omega)$. For our problem under consideration we use

$$\langle R(T), w \rangle := \int_\Omega \left((1 - \eta)\sigma(x, T, |\nabla\varphi|)|\nabla\varphi|^2 + T\right) w \, \mathrm{d}x + \int_\Gamma \kappa(T_a - T)w \, \mathrm{d}\Gamma, \quad w \in W^{1,(q^*)'}(\Omega).$$

Therefore we find a $c_{q^*} > 0$ such that $T \in W^{1,q^*}(\Omega)$ and $\|T\|_{W^{1,q^*}} \le c_{q^*}$.

4. The continuous embedding of $W^{1,q^*}(\Omega)$ into $C(\overline{\Omega})$ supplies the point-wise lower and upper bound of the temperature distribution T which sharpens the result of Step 1. $\qquad\square$

Let us mention that according to the proof of Lemma 4.1, the upper and lower bounds of the electrostatic potential φ of any solution to (P) are given by the upper and lower bound of the Dirichlet function φ^D, respectively. The continuous embedding $W^{1,r}(\Omega) \hookrightarrow C^{0,\alpha}(\overline{\Omega})$ for $r > 2$ in two spatial dimensions ensures the following regularity for solutions to (P).

Corollary 4.2 *We assume (A). Then any solution (φ, T) to (P) is Hölder continuous.*

Theorem 4.2 (Existence of solutions) *We assume (A) and $\eta \in L^\infty(\Omega)$, $\eta(x) \in [0, 1]$ for a.a. $x \in \Omega$. Then there exists at least one solution to Problem (P).*

Proof. 1. We intend to use Schauder's fixed point theorem. We fix q° with $2 < q^\circ < q^*$ and denote by $c_{q^\circ} = c_{q^*,q^\circ} c_{q^*} > 0$ the product of the imbedding constant $c_{q^*,q^\circ} > 0$ of the continuous imbedding $W^{1,q^*}(\Omega) \hookrightarrow W^{1,q^\circ}(\Omega)$ and of the constant c_{q^*} from Theorem 4.1. We work with the bounded, closed, convex, nonempty set

$$\mathcal{M} := \left\{ T \in W^{1,q^\circ}(\Omega) : \|T\|_{W^{1,q^\circ}} \leq c_{q^\circ}, \ T \geq T_a \right\}.$$

On $\mathcal{M}$ we consider the mapping $Q : \mathcal{M} \to \mathcal{M}$, which is defined as follows: For a given $\widetilde{T} \in \mathcal{M}$ we solve problem (4.8), see Lemma 4.1, and get a unique solution φ which possesses the higher regularity $\varphi \in W^{1,p^*}(\Omega)$, see Lemma 4.2. Corollary 4.1 ensures that $(1-\eta)\sigma(x, \widetilde{T}, |\nabla\varphi|)|\nabla\varphi|^2 \in L^{s^*}(\Omega)$. Now we find the unique solution T of the heat flow equation with the right hand side $(1-\eta)\sigma(x, \widetilde{T}, |\nabla\varphi|)|\nabla\varphi|^2 \in L^{s^*}(\Omega) \subset H^1(\Omega)^*$, where $s^* > 1$. This is possible since the corresponding operator $B : H^1(\Omega) \to H^1(\Omega)^*$,

$$\langle BT, w \rangle = \int_\Omega \lambda \nabla T \cdot \nabla w \, \mathrm{d}x + \int_\Gamma \kappa T w \, \mathrm{d}\Gamma, \quad w \in H^1(\Omega),$$

is Lipschitz continuous and strongly monotone from $H^1(\Omega)$ to $H^1(\Omega)^*$ (compare Assumption (A)), which proves the solvability. The higher regularity of the solution is guaranteed by the regularity result of Gröger for second order elliptic equations with nonsmooth data in the two-dimensional case (see [15]). Note that the Joule heating term belongs to $L^{s^*}(\Omega) \subset W^{1,(q^*)'}(\Omega)^*$. Arguing as in Step 3 of the proof of Theorem 4.1 we find that $\|T\|_{W^{1,q^*}} \leq c_{q^*}$. By the continuous imbedding $W^{1,q^*}(\Omega) \hookrightarrow W^{1,q^\circ}(\Omega)$ this results in $\|T\|_{W^{1,q^\circ}} \leq c_{q^*,q^\circ}\|T\|_{W^{1,q^*}} \leq c_{q^\circ}$. Moreover, $T \geq T_a$ is verified similar to the proof of Theorem 4.1. By this procedure the mapping Q is defined by $T := Q(\widetilde{T})$. To apply Schauder's fixed point theorem, we show that $Q : \mathcal{M} \to \mathcal{M}$ is continuous as well as compact.

2. We start with the continuity: Let $\widetilde{T}_n \to \widetilde{T}$ in $W^{1,q^\circ}(\Omega)$ and $\varphi_n, \varphi \in W^{1,p}(\Omega)$ the corresponding solutions to (4.8). The test of (4.8) by $\varphi_n - \varphi \in W_0^{1,p}(\Omega \cup \Gamma_N)$ gives

$$\int_\Omega \sigma_0 F(\cdot, \widetilde{T}_n)\left(|\nabla\varphi_n|^{p-2}\nabla\varphi_n - |\nabla\varphi|^{p-2}\nabla\varphi\right) \cdot \nabla(\varphi_n - \varphi) \, \mathrm{d}x$$

$$= \int_\Omega \sigma_0\left(F(\cdot, \widetilde{T}) - F(\cdot, \widetilde{T}_n)\right)|\nabla\varphi|^{p-2}\nabla\varphi \cdot \nabla(\varphi_n - \varphi) \, \mathrm{d}x.$$

We use (4.5), $\sigma_0 F(\widetilde{T}_n) \geq \sigma_1$, the Lipschitz continuity of F for arguments $T \geq T_a$ and Hölder's inequality to obtain

$$\sigma_1 \int_\Omega |\nabla(\varphi_n - \varphi)|^p \, \mathrm{d}x \leq c \int_\Omega |\widetilde{T}_n - \widetilde{T}||\nabla\varphi|^{p-1}|\nabla(\varphi_n - \varphi)| \, \mathrm{d}x$$
$$\leq c \, \|\widetilde{T}_n - \widetilde{T}\|_{L^\infty} \|\nabla\varphi\|_{L^p}^{p-1} \|\nabla(\varphi_n - \varphi)\|_{L^p}.$$

The continuous imbedding $W^{1,q^\circ}(\Omega) \hookrightarrow L^\infty(\Omega)$ and Lemma 4.1 thus ensure

$$\|\nabla(\varphi_n - \varphi)\|_{L^p}^{p-1} \leq c \, \|\widetilde{T}_n - \widetilde{T}\|_{L^\infty} \to 0. \tag{4.12}$$

Since $\varphi_n - \varphi \in W_0^{1,p}(\Omega \cup \Gamma_N)$ this means that $\|\varphi_n - \varphi\|_{W^{1,p}} \to 0$. Let be $\widehat{p} \in (p, p^*)$ with $\frac{1}{\widehat{p}} = \frac{\theta}{p} + \frac{1-\theta}{p^*}$. By interpolation we get

$$\|\varphi_n - \varphi\|_{L^{\widehat{p}}} \leq \|\varphi_n - \varphi\|_{L^p}^\theta \|\varphi_n - \varphi\|_{L^{p^*}}^{1-\theta} \quad,$$
$$\|\nabla(\varphi_n - \varphi)\|_{L^{\widehat{p}}} \leq \|\nabla(\varphi_n - \varphi)\|_{L^p}^\theta \|\nabla(\varphi_n - \varphi)\|_{L^{p^*}}^{1-\theta}.$$

And since $\|\varphi_n\|_{W^{1,p^*}}$, $\|\varphi\|_{W^{1,p^*}} \leq c_{p^*}$ we thus obtain $\varphi_n \to \varphi$ in $W^{1,\widehat{p}}(\Omega)$ for all $\widehat{p} < p^*$.

Let T_n and T denote the solutions to the heat flow equation with the arguments $(\widetilde{T}_n, \varphi_n)$ and $(\widetilde{T}, \varphi)$ in the Joule heating term, respectively. We test these equations by $T_n - T$. Taking into account Assumption (A), we find

$$\|T_n - T\|_{H^1}^2$$
$$\leq c \int_\Omega \left(F(\cdot, \widetilde{T}_n)|\nabla\varphi_n|^p - F(\cdot, \widetilde{T})|\nabla\varphi|^p \right)|T_n - T| \, \mathrm{d}x \tag{4.13}$$
$$\leq c \int_\Omega \left(F(\cdot, \widetilde{T}_n)\big||\nabla\varphi_n|^p - |\nabla\varphi|^p\big| + |\nabla\varphi|^p|F(\cdot, \widetilde{T}_n) - F(\cdot, \widetilde{T})|\right)|T_n - T| \, \mathrm{d}x.$$

By the vector inequality (see [20, p. 379] or [2, Chap. 4, p. 257])

$$\big||y|^{p-2}y - |z|^{p-2}z\big| \leq 3(p-1)|y - z|(|y| + |z|)^{p-2} \quad \text{for } p \geq 2, \quad y, z \in \mathbb{R}^n$$

we derive

$$\big||y|^p - |z|^p\big| \leq \big||y|^{p-2}y \cdot y - |z|^{p-2}z \cdot z\big|$$
$$\leq |y|\big||y|^{p-2}y - |z|^{p-2}z\big| + \big||z|^{p-2}z\big||y - z|$$
$$\leq c(p)|y - z|(|y| + |z|)^{p-1}.$$

Applying this inequality and using the boundedness and the Lipschitz continuity of F for second arguments greater or equal to T_a we continue the estimate (4.13) by

$$\|T_n - T\|_{H^1}^2 \leq c \int_\Omega \left(c(p)|\nabla\varphi_n - \nabla\varphi|(|\nabla\varphi_n| + |\nabla\varphi|)^{p-1} + |\nabla\varphi|^p|\widetilde{T}_n - \widetilde{T}|\right)|T_n - T| \, \mathrm{d}x$$
$$\leq \widetilde{c}(p)\|\nabla(\varphi_n - \varphi)\|_{L^{\widehat{p}}}\left(\|\varphi_n\|_{W^{1,p^*}}^{p-1} + \|\varphi\|_{W^{1,p^*}}^{p-1}\right)\|T_n - T\|_{L^q}$$
$$+ \widetilde{c}(p)\|\varphi\|_{W^{1,p^*}}^p\|\widetilde{T}_n - \widetilde{T}\|_{L^\infty}\|T_n - T\|_{L^{\widetilde{q}}},$$

where p^* is defined in Lemma 4.2 and

$$\widehat{p} \in (p, p^*), \quad \frac{1}{\widehat{p}} + \frac{p-1}{p^*} + \frac{1}{q} = 1, \quad \frac{1}{\widetilde{q}} + \frac{p}{p^*} = 1.$$

Note that $\|\varphi_n\|_{W^{1,p^*}}$, $\|\varphi\|_{W^{1,p^*}} \leq c_{p^*}$ and $\|T_n - T\|_{L^q} \leq c(q)\|T_n - T\|_{H^1}$, $\|T_n - T\|_{L^{\widetilde{q}}} \leq c(\widetilde{q})\|T_n - T\|_{H^1}$ as well as $\|\widetilde{T}_n - \widetilde{T}\|_{L^\infty}$, $\|\nabla(\varphi_n - \varphi)\|_{L^{\widehat{p}}} \to 0$. Thus, in summary we obtain

$$\|T_n - T\|_{H^1} \to 0.$$

Since $\|T_n\|_{W^{1,q^*}}$, $\|T\|_{W^{1,q^*}} \leq c_{q^*}$ this convergence implies by interpolation arguments the convergence $T_n \to T$ in $W^{1,q^\circ}(\Omega)$ since $2 < q^\circ < q^*$.

3. To show that Q is compact we start with any sequence $(\widetilde{T}_n)$, $\widetilde{T}_n \in \mathcal{M}$. Since $\mathcal{M}$ is bounded in $W^{1,q^\circ}(\Omega)$ and $W^{1,q^\circ}(\Omega)$ is compactly embedded in $L^\infty(\Omega)$ we find a $\widetilde{T} \in L^\infty(\Omega)$ and a subsequence (also denoted by $(\widetilde{T}_n)$) such that $\widetilde{T}_n \to \widetilde{T}$ in $L^\infty(\Omega)$. Therefore, we can argue as in Step 2 of the proof to verify that $Q\widetilde{T}_n \to Q\widetilde{T}$ in $W^{1,q^\circ}(\Omega)$. Thus Schauder's fixed point theorem proves the theorem. $\quad\square$

5 Conclusions, remarks, generalizations, and open problems

5.1 Electrothermal description of organic thin film devices

In all organic devices with sufficiently large activation energies, self-heating can lead to S-shaped current-voltage characteristics with NDR regions and can promote spatial inhomogeneities. To address this issue, we introduced a PDE thermistor model for the study of the appearance and the evolution of spatially local NDR regions in large-area thin film devices in dependence on the applied voltage. The model equations (3.1) – (3.4) include the positive temperature feedback by an Arrhenius law for the conductivity and the non-Ohmic setting.

We presented a finite-volume scheme for the PDE system (3.1) – (3.4) which is able to reveal regions of NDR and "switched back" regions in the device. Moreover, we verified that the network model used in [11] can be interpreted as a finite-volume discretization of (3.1) – (3.4) under additional assumptions on the device geometry.

NDR phenomena in OLEDs are already present at moderate temperature rises and are the reason for an accelerated increase in brightness inhomogeneities. Our studies can help to elucidate spatial inhomogeneities of current density and luminance in large-area lighting panels at high power.

5.2 Analysis for the thermistor model with p-Laplace and Arrhenius-like temperature law in the conductivity

We studied the model (4.1a) – (4.2b) in two spatial dimensions for the organic material, where $p > 2$ has to be assumed. The heat transfer through the glass substrate and the contacts is substituted by a boundary condition of third kind. The voltage drop in the

ITO contact is described by a decreasing Dirichlet value for the electrostatic potential φ depending on the distance to the additional metal contact at the side (see Fig. 2 left).

In two spatial dimensions we gave a weak formulation of the problem, derived a priori bounds for the solutions and their derivatives and finally proved the existence of a weak solution for this non-standard thermistor problem. Here, the theory of monotone operators and the higher regularity results of [10] for the p-Laplace were important ingredients.

Open questions remain concerning the extension of the analytical treatment of the problem in the following directions: (i) Results in three spatial dimensions require further regularity results for the p-Laplace expressions. (ii) The model complexity could include a dependence of the external power efficiency η on the temperature T and the current $\vec{j}$. This relation can be obtained from fitting data resulting from measurements. (iii) Instead of the stationary thermistor problem (4.1a) – (4.2b) one can consider the evolution problem consisting of the parabolic heat flow equation together with the self-consistently calculated electrostatic potential to describe the self-heating effects during the time being.

5.3 Including ITO layer and glass substrate in the analytical treatment

The ITO layer has an Ohmic current-voltage relation and no temperature activated conductivity law. If this part of the structure should be included in the simulation domain, a heterostructure with varying exponent p has to be considered. A varying p arises also, if various layers of different organic material have to be described. An overview concerning the analytical treatment of problems including the $p(x)$-Laplacian (varying p over the considered domain) is given in [16]. For suited function spaces see [6, 7]. Regularity issues for problems with $p(x)$ growth (needed in the analytical treatment of the Joule heating term comp. Lemma 4.2) are addressed in [8] assuming a certain modulus of continuity. A series of analytic tools is available for log-Hölder continuous exponents $p(x)$, see [6]. However, in our situation the exponents p are large ($p \approx 10$) in the organic OLED materials and jump to $p = 2$ in the Ohmic ITO subdomain. Here, the large variation of p is a particular challenge in the mathematical treatment of the model system.

To include also the heat transfer through the glass substrate (see the Fig. 2 left) which is expressed in our model equations (3.1) – (3.4) only by a boundary condition of third kind, one has to enlarge the domain of simulation. The electrical equation has to be fulfilled on the same domain as before, but the heat flow equation lives on a domain which additionally contains the area of the glass substrate and boundary conditions have to be formulated for the heat transfer to the air at the new boundary.

References

[1] K. J. Bergemann, R. Krasny, and S. R. Forrest, *Thermal properties of organic light-emitting diodes*, Organic Electronics **13** (2012), no. 9, 1565–1568.

[2] N. Bourbaki, *Éléments de mathématique. Fasc. XIII. Livre VI: Intégration. Chapitres 1, 2, 3 et 4: Inégalités de convexité, Espaces de Riesz, Mesures sur les espaces localement compacts, Prolongement d'une mesure, Espaces L^p*, Deuxième édition revue et augmentée. Actualités Scientifiques et Industrielles, No. 1175, Hermann, Paris, 1965.

[3] A. Bradji and R. Herbin, *Discretization of coupled heat and electrical diffusion problems by finite-element and finite-volume methods*, IMA Journal of Numerical Analysis **28** (2008), no. 3, 469–495.

[4] G. Cimatti, *Remark on existence and uniqueness for the thermistor problem under mixed boundary conditions*, Quart. Appl. Math. **47** (1989), no. 1, 117–121.

[5] ———, *A remark on the thermistor problem with rapidly growing conductivity*, Appl. Anal. **80** (2001), no. 1-2, 133–140.

[6] L. Diening, P. Harjulehto, P. Hästö, and M. Růžička, *Lebesgue and Sobolev spaces with variable exponents*, Lecture Notes in Mathematics, vol. 2017, Springer, Heidelberg, 2011.

[7] L. Diening, P. Nägele, and M. Růžička, *Monotone operator theory for unsteady problems in variable exponent spaces*, Complex Var. Elliptic Equ. **57** (2012), no. 11, 1209–1231.

[8] M. Eleuteri, *Hölder continuity results for a class of functionals with non standard growth*, Artic. Ric. Mat. **7** (2004), no. 8, 129–157.

[9] R. Eymard, T. Gallouët, and R. Herbin, *Finite volume methods*, Handbook of numerical analysis, Vol. VII, Handb. Numer. Anal., VII, North-Holland, Amsterdam, 2000, pp. 713–1020.

[10] A. Fiaschi, D. Knees, and S. Reichelt, *Global higher integrability of minimizers of variational problems with mixed boundary conditions*, J. Math. Anal. Appl. **401** (2013), no. 1, 269–288.

[11] A. Fischer, T. Koprucki, K. Gärtner, M. L. Tietze, J. Brückner, B. Lüssem, K. Leo, A. Glitzky, and R. Scholz, *Feel the heat: Nonlinear electrothermal feedback in organic LEDs*, Adv. Funct. Mater. **24** (2014), no. 22, 3366–3366.

[12] A. Fischer, P. Pahner, B. Lüssem, K. Leo, R. Scholz, T. Koprucki, J. Fuhrmann, K. Gärtner, and A. Glitzky, *Self-heating effects in organic semiconductor crossbar structures with small active area*, Organic Electronics **13** (2012), no. 11, 2461–2468.

[13] A. Fischer, P. Pahner, B. Lüssem, K. Leo, R. Scholz, T. Koprucki, K. Gärtner, and A. Glitzky, *Self-heating, bistability, and thermal switching in organic semiconductors*, Phys. Rev. Lett. **110** (2013), 126601.

[14] H. Gajewski, K. Gröger, and K. Zacharias, *Nichtlineare Operatorgleichungen und Operatordifferentialgleichungen*, Akademie-Verlag, Berlin, 1974, Mathematische Lehrbücher und Monographien, II. Abteilung, Mathematische Monographien, Band 38.

[15] K. Gröger, *A $W^{1,p}$-estimate for solutions to mixed boundary value problems for second order elliptic differential equations*, Math. Ann. **283** (1989), no. 4, 679–687.

[16] P. Harjulehto, P. Hästö, Út V. Lê, and M. Nuortio, *Overview of differential equations with non-standard growth*, Nonlinear Anal. **72** (2010), no. 12, 4551–4574.

[17] A. Ü. Keskin, *A simple analog behavioural model for NTC thermistors including self-heating effect*, Sensors and Actuators A: Physical **118** (2005), no. 2, 244–247.

[18] Z. Kohári and L. Pohl, *How thermal environment affects OLEDs' operational characteristics*, 28 th IEEE SEMI-THERM Symposium, 2012, p. 331.

[19] P. Lindqvist, *Notes on the p-Laplace equation*, Report. University of Jyväskylä Department of Mathematics and Statistics, vol. 102, University of Jyväskylä, Jyväskylä, 2006.

[20] D. S. Mitrinović, *Analytic inequalities*, Springer-Verlag, New York-Berlin, 1970, In cooperation with P. M. Vasić. Die Grundlehren der mathematischen Wissenschaften, Band 165.

[21] J. Park, J. Lee, and Y. Noh, *Optical and thermal properties of large-area OLED lightings with metallic grids*, Org. Electron. **13** (2012), 184–194.

[22] L. Pohl and E. Kollar, *Extension of the sunred algorithm for electrothermal simulation and its application in failure analysis of large area (organic) semiconductor devices*, THERMINIC 17th Workshop on thermal investigation of ICs and Systems, Sept. 2011, Paris, 2011, pp. 1–6.

[23] E. Schöll, *Nonequilibrium phase transitions in semiconductors: Self- organization induced by generation and recombination processes*, Springer Series in Synergetics, Springer-Verlag, 1987.

[24] M. P. Shaw, V. V. Mitin, E. Schöll, and H. L. Grubin, *The physics of instabilities in solid state electron devices*, Plenum Press, New York, 1992.

[25] M. Slawinski, D. Bertram, M. Heuken, H. Kalisch, and A. Vescan, *Electrothermal characterization of large-area organic light-emitting diodes employing finite-element simulation*, Organic Electronics **12** (2011), no. 8, 1399–1405.

[26] M. Slawinski, M. Weingarten, M. Heuken, A. Vescan, and H. Kalisch, *Investigation of large-area OLED devices with various grid geometries*, Organic Electronics **14** (2013), no. 10, 2387–2391.

[27] S. L. M. van Mensfoort and R. Coehoorn, *Effect of Gaussian disorder on the voltage dependence of the current density in sandwich-type devices based on organic semiconductors*, Phys. Rev. B **78** (2008), 085207.

[28] Hong Xie and W. Allegretto, $C^\alpha(\overline{\Omega})$ *solutions of a class of nonlinear degenerate elliptic systems arising in the thermistor problem*, SIAM J. Math. Anal. **22** (1991), no. 6, 1491–1499.

[29] L. Yang, B. Wei, and J. Zhang, *Transient thermal characterization of organic light-emitting diodes*, Semiconductor Science and Technology **27** (2012), no. 10, 105011.

[30] E. Zeidler, *Nonlinear functional analysis and its applications. II/B*, Springer-Verlag, New York, 1990, Nonlinear monotone operators, Translated from the German by the author and Leo F. Boron.